

GAMMA: Generalizable Alignment via Multi-task and Manipulation-Augmented Training for AI-Generated Image Detection

Haozhen Yan¹, Yan Hong², Suning Lang¹, Jiahui Zhan¹, Yikun Ji¹, Yujie Gao¹,
Jun Lan², Huijia Zhu², Weiqiang Wang², Jianfu Zhang^{1,*}

¹Shanghai Jiao Tong University

²Ant Group

orion810@sjtu.edu.cn c.sis@sjtu.edu.cn

Abstract

With generative models becoming increasingly sophisticated and diverse, detecting AI-generated images has become increasingly challenging. While existing AI-generated Image detectors achieve promising performance on in-distribution generated images, their generalization to unseen generative models remains limited. This limitation is largely attributed to their reliance on generation-specific artifacts, such as stylistic priors and compression patterns. To address these limitations, we propose **GAMMA**, a novel training framework designed to reduce domain bias and enhance semantic alignment. GAMMA introduces diverse manipulation strategies, such as inpainting-based manipulation and semantics-preserving perturbations, to ensure consistency between manipulated and authentic content. We employ multi-task supervision with dual segmentation heads and a classification head, enabling pixel-level source attribution across diverse generative domains. In addition, a reverse cross-attention mechanism is introduced to allow the segmentation heads to guide and correct biased representations in the classification branch. Our method achieves state-of-the-art generalization performance on the GenImage benchmark, improving accuracy by 5.8%, but also maintains strong robustness on newly released generative model such as GPT-4o.

1 Introduction

The rapid advancement of generative models (Ho, Jain, and Abbeel 2020; Rombach et al. 2022) has dramatically revolutionized the landscape of synthetic content creation. Leveraging powerful pretrained architectures and intuitive prompt-based interfaces, users without technical expertise can now easily generate high-fidelity images. This accessibility has raised growing concerns regarding misuse, content authenticity, and intellectual property violations (Epstein, Hertzmann et al. 2023). One technical approach to detecting AI-generated images is digital watermarking (Zhang et al. 2024), which embeds imperceptible features during image generation for later identification. However, watermarking cannot be enforced in open settings (e.g., open-source models), and is thus more suited for controlled scenarios like copyright protection than for general content authenticity verification. In more general scenarios, detectors are expected to determine whether an image is AI-generated

solely from visual cues. Although impressive performance has been reported on in-distribution benchmarks, generalization to unseen generative models remains fundamentally limited. This performance gap is well-documented in previous work, and has been attributed to several key factors: image storage formats (Grommelt et al. 2025), degradation from resizing or blurry (Li et al. 2025), the limitations of binary classification objectives (Yan et al. 2025c), and dataset bias (Guillaro et al. 2025). These limitations highlight the need for a new training paradigm that goes beyond binary classification and handcrafted artifacts. Specifically, detectors must learn to recognize the *structural and semantic inconsistencies* characteristic of synthetic content, rather than memorizing dataset-specific features or model-specific noise.

To address the limited generalization of detectors, we propose **GAMMA**, a novel training framework designed to reduce dataset bias and enhance semantic alignment.

Semantically Aligned Manipulation Diversity. To enhance semantic consistency and manipulation diversity, we employ multiple content-aligned forgeries, including inpainting, inpainting-blended variants, Copy-Move and Splicing artifacts, shown in Fig. 2. We leverage the COCO-Inpaint dataset (Yan et al. 2025a) for diverse inpainting settings and generate an inpainting-blended dataset by restoring original backgrounds, isolating subtle artifacts in unmasked regions.

Cheat operations (Copy-Move and Splicing) inconsistencies further enrich our manipulation suite. This diversified forgery portfolio mitigates distributional biases and yields more robust forensic representations. Our diversified, content-aligned forgery portfolio provides high-level semantic alignment, mitigating distributional biases between authentic and generated images and yielding more robust forensic representations.

Multi-Task Fine-Grained Supervision. To fully leverage the introduced locally manipulated data, two auxiliary segmentation heads are employed to provide fine-grained supervision by explicitly learning the origin of each pixel. The Manipulation Segmentation head differentiates any altered pixel from genuine content, whereas the AI Segmentation head exclusively pinpoints pixels synthesized by AI models. This fine-grained guidance steers the classification head toward discriminative artifact regions and avoids the

*Corresponding authors.

low-rank feature collapse induced by vanilla binary objectives (Yan et al. 2025c). In addition, decoupling generic tampering from AI-specific synthesis enhances the robustness and specialization of the AI Segmentation head. Furthermore, even when segmentation heads reveal subtle artifact cues, the classification head can still misclassify highly realistic AI-generated images, such as those produced by GPT4o (Open AI 2025). To eliminate this inconsistency, we introduce a reverse cross-attention mechanism that enables the segmentation branch to rectify potentially biased classification predictions.

Finally, we validate the effectiveness of GAMMA through comprehensive experiments across a range of benchmarks. GAMMA achieves state-of-the-art generalization on Gen-Image (Zhu et al. 2023) (improving accuracy by 5.4% over prior best method) while maintaining strong adaptability to newly released Multimodal Large Language Models like GPT-4o (Open AI 2025). We further evaluate GAMMA’s robustness under common degradation scenarios (e.g., JPEG compression), demonstrating superior resistance to real-world perturbations.

2 Related Works

2.1 Low-Level Detection Methods

Initial research efforts concentrated on identifying images synthesized by GAN architectures (Karras, Laine, and Aila 2019; Choi et al. 2018), with detection models predominantly based on convolutional neural networks (CNNs). Zhang (2019) demonstrated that GAN-generated images exhibit distinctive artifacts in the frequency domain, specifically spectral duplication, which can be exploited for detection. However, subsequent studies (Ricker et al. 2024; Corvi et al. 2023; Karageorgiou et al. 2025) have shown that such artifacts are not as pronounced in dominant diffusion generated images. Some recent works also utilize frequency-domain information, typically by introducing spectrum representations as an auxiliary branch. AIDE (Yan et al. 2025b) combines CLIP-based (Radford et al. 2021) semantic embeddings with frequency-aware patch-level artifact analysis. SPAI (Karageorgiou et al. 2025) models forensic microstructures and spectral distributions of real images in a self-supervised manner, enabling zero-shot detection of AI-generated images via residual learning and spectral reconstruction divergence. These low-level methods are sensitive to image degradation, as the extracted features are easily disrupted, leading to reduced detection performance. Moreover, they exhibit limited robustness against adversarial attacks.

2.2 Reconstruction-based Detection Methods

Reconstruction-based methods are primarily inspired by the pioneering work of DIRE (Wang et al. 2023). The central hypothesis of DIRE is that images generated by diffusion models can be more accurately reconstructed by a pre-trained diffusion model than real images. This reconstruction discrepancy is leveraged as a signal for detecting synthetic content. Subsequent works have built upon this idea, exploring various reconstruction techniques and architectures. DRCT (Chen et al. 2024a) generates hard sam-

ples via diffusion reconstruction and leverages contrastive learning to guide the learning of reconstruction residuals. AEROBLADE (Ricker, Lukovnikov, and Fischer 2024) discards the diffusion reconstruction process and instead utilizes VAE (Kingma and Welling 2014) for image reconstruction. The second-layer features from the LPIPS (Zhang et al. 2018) are then extracted and used as discriminative statistics for detection. FakeInversion (Cazenavette et al. 2024) enhances its reconstruction-based detection by using reverse image search to retrieve real images that match each generated sample. However, such reconstruction-based cues are vulnerable to lossy compression artifacts, particularly those introduced by JPEG encoding (Grommelt et al. 2025; Ricker, Lukovnikov, and Fischer 2024). Moreover, diffusion-based reconstruction adds significant computational overhead during both training and inference.

Reconstruction-based methods provide a degree of semantic alignment, but inpainting maintains stylistic coherence by exploiting local context from unmask regions while full-image inversion operates without such guidance and can introduce style mismatches.

2.3 Content-consistency training strategy

While earlier efforts mainly centered on algorithmic advances, recent research has increasingly shifted toward improving dataset quality to strengthen semantic alignment between real and generated images. B-Free (Guillaro et al. 2025) performs content augmentation via inpainting to achieve semantic alignment between authentic and generated images. Specifically, The COCO (Lin et al. 2014) images are used as real references, while segmentation masks guide Stable Diffusion 2.1 (Rombach et al. 2022) to inpaint segmentation regions, resulting in locally manipulated AI-generated images. COCO-Inpaint (Yan et al. 2025a) adopts a broader range of inpainting models and more diverse mask generation strategies, incorporating both text-guided and text-unguided settings to produce more generalizable inpainted images. It also emphasizes the importance of randomly generated masks to decouple object-centric regions from manipulated areas, thereby reducing the risk of detectors relying on spatial priors rather than genuine manipulation cues. MaskCLIP (Wang, Huang, and Hong 2025) simulates user edits by leveraging VLMs (AI 2024; Liu et al. 2023; Chen et al. 2024b; Wang et al. 2024) to generate editing prompts, employs segmentors (Kirillov et al. 2023; Xiao et al. 2024) to localize target regions, and performs inpainting using SD-based diffusion models.

Relying solely on semantic alignment within a binary classification framework is insufficient to ensure generalization. Effort in (Yan et al. 2025c) demonstrated such objectives can constrain the feature space to a low-rank structure and cause detectors to overfit to limited fake patterns. Models must focus on generative artifacts like diffusion noise patterns, spectral anomalies, and microstructural traces instead of superficial distributional shortcuts.

3 Methodology

To address the limitations of binary supervision and restricted feature diversity, we design a unified training frame-

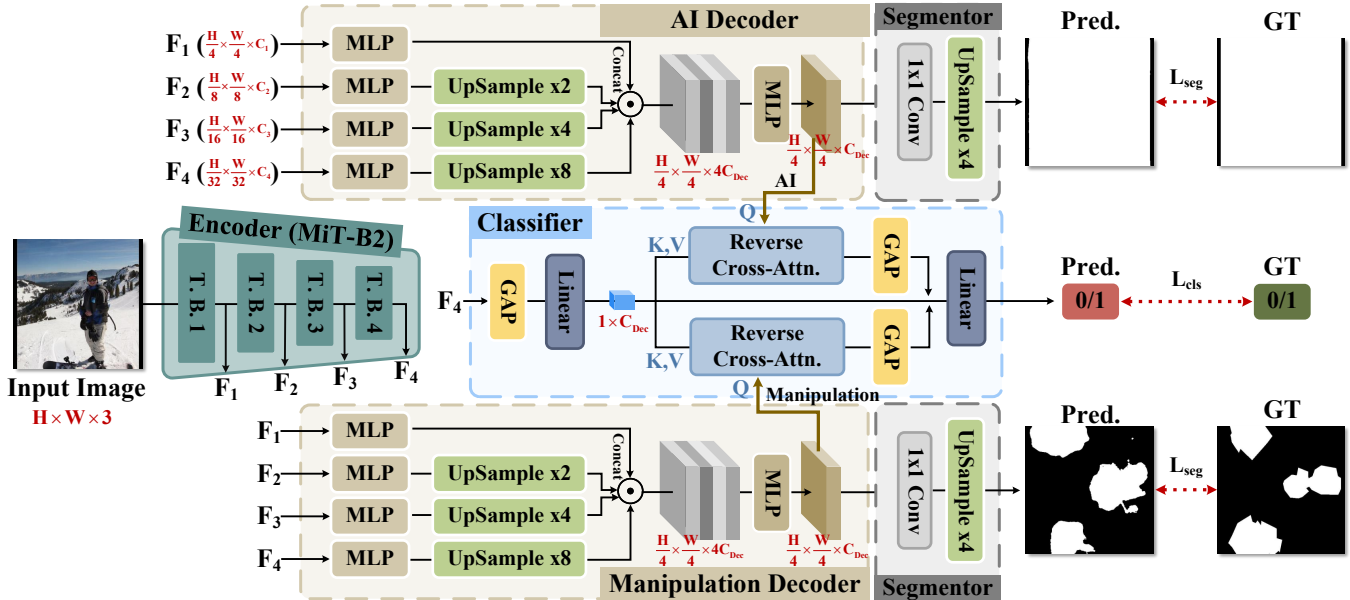


Figure 1: The Overview of GAMMA. Given an input image $\mathbf{I} \in \mathbb{R}^{H \times W \times 3}$, multi-scale features \mathbf{F}_i are extracted via the MiT-B2 encoder and unified through MLP projection and upsampling. Two parallel decoders with identical architectures yield decoder outputs $\mathbf{F}_{\text{Dec}}^{AI}$ and $\mathbf{F}_{\text{Dec}}^{Ma}$, where $\mathbf{F}_{\text{Dec}} \in \mathbb{R}^{\frac{H}{4} \times \frac{W}{4} \times C_{\text{Dec}}}$; while the classifier predicts the global authenticity label with the aid of **Reverse Cross-Attention**, enabling the segmentation branches to rectify potentially biased classification responses (Figure 3).

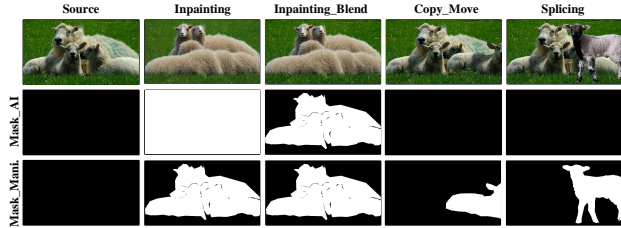


Figure 2: Different manipulation categories. In inpainting, unmasked regions also pass through diffusion and induces subtle pixel changes, yielding an all-white Mask_AI.

work that enhances generalization through diverse manipulations and multi-task learning. The proposed approach is structured around three key components, detailed below. An overview of the entire framework is illustrated in Figure 1.

3.1 Format Alignment

Following prior works (Grommelt et al. 2025; Ricker, Lukovnikov, and Fischer 2024), to address format bias, we re-encode all PNG-stored generated images into JPEG using a quality factor of 96, consistent with the JPEG compression applied in ImageNet (Deng et al. 2009). This process ensures that the format of generated images aligns with that of real images, thereby mitigating the risk of detectors relying on superficial format cues.

3.2 Semantically Aligned Manipulation Diversity

To ensure semantic consistency while enriching the diversity of manipulations, multiple types of image forgeries aligned with the original content are incorporated. Visualizations of the various manipulation types are shown in Figure 2 and Figure 5.

Inpainting. COCO-Inpaint (Yan et al. 2025a) is adopted as our inpainting dataset; it includes multiple inpainting models, mask generation schemes, and both text-guided and unguided modes, whose combinatorial configurations yield extensive diversity and realism.

Inpainting-Blended. Although inpainting models are conditioned on explicit masks, the unmasked regions in the output images are regenerated through the diffusion process. To preserve the authenticity of unmasked content, we blend it with the original image by pasting the unmasked area to the inpainted images, resulting in a refined dataset variant called COCO-Inpainted-Blended.

Copy-Move and Splicing. While inpainting creates localized manipulations that enable pixel-level supervision, relying on a single binary segmentation head risks biased feature learning. To improve robustness, we introduce low-cost manipulations such as Copy-Move and Splicing, which involve rearranging real pixels without introducing AI-generated content. These manipulations compel the model to learn structural inconsistencies, improving its generalization to more subtle manipulations. Specifically, we incorporate these two manipulation types from the corresponding subsets of the TampCOCO dataset (Kwon et al. 2022).

Training Dataset	#Sample	Cls.	Seg.			
			Mani.		AI	
			Background	Foreground	Background	Foreground
COCO (Lin et al. 2014)	117,266	0	0	0	0	0
COCO-Inpaint (Yan et al. 2025a)	258,266	1	0	1	1	1
COCO-Inpaint-Blended	258,266	1	0	1	0	1
TampCOCO-CopyMove (Kwon et al. 2022)	200,000	0	0	1	0	0
TampCOCO-Splicing (Kwon et al. 2022)	200,000	0	0	1	0	0

Table 1: Label for Training Dataset. 0 indicates authentic, 1 indicates manipulated or AI-generated.

3.3 Multi-Task Fine-Grained Supervision

While a unified pixel-level segmentation head can detect generic manipulations, different forgery types often exhibit distinct visual cues and semantic inconsistencies. To capture these heterogeneous patterns more effectively, we employ a multi-task supervision strategy by introducing separate segmentation heads for distinct manipulation types. Specifically, we introduce two task-specific segmentation heads:

AI segmentation head. Trained to identify pixels generated by AI-based models.

Manipulation segmentation head. Trained to predict whether each pixel has undergone any form of manipulation.

The two segmentation heads serve complementary purposes: The Manipulation segmentation head encourages the model to localize general manipulations regardless of their source, while the AI segmentation head explicitly focuses on artifacts unique to AI-generated content, such as stylistic inconsistencies and texture patterns. This decoupled supervision guides the backbone to learn both broad manipulation priors and fine-grained generative cues, improving generalization to unseen generative models. Label configurations for classification and segmentation are shown in Table 1. Our classification task aims to distinguish AI-generated images from real ones, based on whether the image contains **pixels synthesized by neural networks**. This definition reflects a fundamental difference between content that is explicitly generated or predicted by models versus content that is merely rearranged from real sources. **COCO-Inpaint** and **COCO-Inpaint-Blended** involve generative inpainting models that directly predict pixel values for masked regions. Hence, these images are labeled as AI-generated. **Tamp-COCO** operate purely with low-cost operations by duplicating existing real pixels without any learned generation. Therefore, they are labeled as real in the classification task.

To achieve accurate mask prediction, we utilize SegFormer (Xie et al. 2021), a transformer-based semantic segmentation model to estimate both manipulation and AI-generated masks from the input image $\mathbf{I} \in \mathbb{R}^{H \times W \times 3}$, and the corresponding manipulation and AI-generated GroundTruth (GT) are denoted as $\mathbf{M}^{Ma} \in \mathbb{R}^{H \times W}$ and $\mathbf{M}^{AI} \in \mathbb{R}^{H \times W}$. The extracted features from the encoder \mathbf{E} at i -th stage are $\mathbf{F}_i = \mathbf{E}(\mathbf{I}) \in \mathbb{R}^{\frac{H}{r_i} \times \frac{W}{r_i} \times C_i}$, where $i \in \{1, 2, 3, 4\}$ and $r_i \in \{4, 8, 16, 32\}$. The multi-scale features \mathbf{F}_i is independently projected to unified channel di-

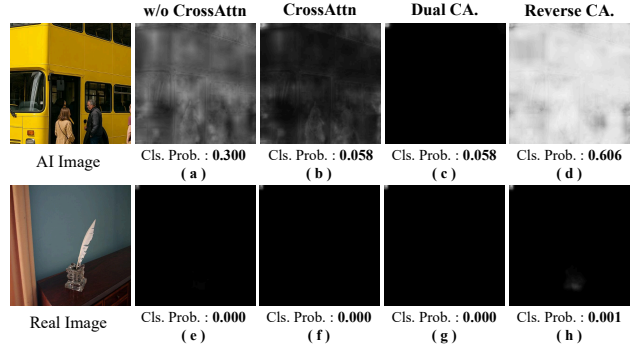


Figure 3: Impact of different Cross Attention (CA.) configurations on segmentation (AI Seg.) and classification performance. Cls. Prob. denotes the predicted probability of the image being AI-generated.

ensions via an MLP:

$$\hat{\mathbf{F}} = \text{MLP}_i(\mathbf{F}_i). \quad (1)$$

Subsequently, lower-resolution features are spatially upsampled to match the resolution of $\hat{\mathbf{F}}_1$:

$$\mathbf{F}_{\text{concat}} = \text{Concat}(\hat{\mathbf{F}}_1, \text{Up}_2(\hat{\mathbf{F}}_2), \text{Up}_4(\hat{\mathbf{F}}_3), \text{Up}_8(\hat{\mathbf{F}}_4)). \quad (2)$$

Finally, the concatenated features are processed by convolutional layers followed by an MLP to yield the decoder output:

$$\mathbf{F}_{\text{Dec}} = \text{MLP}(\text{Conv}(\mathbf{F}_{\text{concat}})) \in \mathbb{R}^{\frac{H}{4} \times \frac{W}{4} \times C_{\text{Dec}}}. \quad (3)$$

AI and Manipulation decoders share the same architectural design. Thus, we obtain two decoder outputs: $\mathbf{F}_{\text{Dec}}^{AI}$, $\mathbf{F}_{\text{Dec}}^{Ma}$. Then, the features \mathbf{F}_{Dec} are passed through a 1×1 convolution to adjust the channel dimension, followed by upsampling to generate the final prediction maps $\hat{\mathbf{M}}$:

$$\hat{\mathbf{M}} = \text{Up}_4(\text{Conv}_{1 \times 1}(\mathbf{F}_{\text{pre}})), \hat{\mathbf{M}} \in \mathbb{R}^{H \times W}. \quad (4)$$

For classification, we apply global pooling (GAP) to the final-layer features \mathbf{F}_4 , followed by a linear projection to obtain a compact representation:

$$\mathbf{F}_{\text{Dec}}^{\text{Cls.}} = \text{Linear}(\text{GAP}(\mathbf{F}_4)) \in \mathbb{R}^{1 \times C_{\text{Dec}}}. \quad (5)$$

Acc↑	GenImage (JPEG-96)								Avg.
	BigGAN	VQDM	ADM	GLIDE	SD 1.4	SD 1.5	Midjourney	Wukong	
CNNDetect	58.4	51.2	49.9	50.7	50.1	49.9	50.1	50.2	51.3
DMID	52.3	75.1	51.3	56.6	99.9	99.8	97.4	99.6	79.0
LGrad	28.9	30.8	30.5	30.0	49.8	49.1	50.6	46.9	39.6
UnivFD	86.1	79.7	64.4	63.9	55.5	56.6	54.2	63.7	65.5
DeFake	64.4	64.4	48.5	80.4	85.1	85.4	79.2	81.8	73.7
DIRE	46.9	47.7	46.7	47.0	47.3	47.3	47.5	47.7	47.3
AntifakePrompt	81.7	81.1	81.6	81.8	77.1	76.6	70.4	77.6	78.5
NPR	56.3	53.9	50.5	48.3	49.4	49.7	47.4	50.2	50.7
FatFormer	80.1	71.5	60.4	65.1	52.0	53.3	51.6	58.1	61.5
FasterThanLies	54.1	76.6	77.2	66.1	92.2	92.3	69.7	88.1	77.0
RINE	88.5	81.4	63.9	74.7	60.5	61.1	52.4	70.0	69.1
AIDE	50.7	51.0	50.1	52.3	74.5	75.9	57.4	69.3	60.2
LaDeDa	80.3	34.8	34.6	34.5	54.8	53.0	52.1	57.7	50.2
C2P-CLIP	87.5	74.1	71.3	74.8	80.5	79.1	55.9	81.0	75.5
CoDE	50.0	56.0	51.9	58.0	96.6	96.5	69.6	95.0	71.7
B-Free	68.7	88.7	79.8	85.3	98.8	98.8	95.7	99.0	89.3
GAMMA (ours)	96.4	91.8	92.5	92.2	97.5	97.0	96.5	97.1	95.1

Table 2: Generalization performance of different methods on the GenImage (JPEG-96).

Acc↑	SynthWildX	OpenAI-4o		GPT-ImgEval	ShareGPT-4o-Image
		T2I	Human Preference		
DMID	48.3		49.8	50.5	50.2
C2P-CLIP	58.2		49.8	49.6	49.1
B-Free	95.6		53.5	57.5	55.5
GAMMA (ours)	99.1		79.4	84.1	70.2

Table 3: Generalization on other generative datasets.

The full training objective is defined as:

$$\mathcal{L} = \alpha(\mathcal{L}_{\text{Cls.}} + \mathcal{L}_{\text{Seg}_{AI}}) + \mathcal{L}_{\text{Seg}_{Ma.}}, \quad (6)$$

where $\alpha = 2$ is a balancing hyper-parameter.

Reverse Cross Attention. We observe that most existing detectors tend to misclassify photorealistic generated images as real. In contrast, segmentation heads can still capture localized manipulation cues in such cases due to their fine-grained spatial sensitivity (Fig. 3(a)). Notably, for authentic images, the segmentation predictions are generally consistent with the classification results (Fig. 3(e-h)). Motivated by this observation, we propose to enhance the interaction between the segmentation and classification branches by introducing a reverse cross-attention mechanism. Specifically, the cross-attention is estimated as:

$$\text{Attention}(Q, K, V) = \text{Softmax} \left(\frac{QK^\top}{\sqrt{d_{\text{head}}}} \right) V, \quad (7)$$

where we set the query Q from the segmentation head \mathbf{F}_{Dec} and the key K and value V from the classification head. The

resulting attention is then residually added back to the classification features:

$$\mathbf{F}_{\text{Dec}}^{\text{Cls.}} = \mathbf{F}_{\text{Dec}}^{\text{Cls.}} + \sum_{t \in \{\text{Ma, AI}\}} \text{Pool}(\text{Attn}(\mathbf{F}_{\text{Dec}}^t, \mathbf{F}_{\text{Dec}}^{\text{Cls.}}, \mathbf{F}_{\text{Dec}}^{\text{Cls.}})). \quad (8)$$

Intuitively, the reverse attention allows the segmentation head to actively reinforce informative cues from the classification representation, providing fine-grained spatial guidance. This mechanism effectively enables the segmentation branch to rectify potentially biased classification responses (Fig. 3(d)). In contrast, the standard cross-attention, where the classifier serves as the query, may propagate the classification bias further (Fig. 3(b)). Although dual cross-attention incorporates bidirectional attention into the classification feature, it introduces interference due to semantic inconsistency between the AI-generated and manipulation branches.

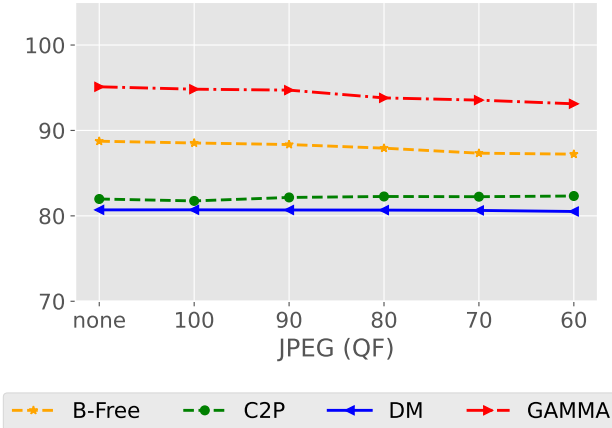


Figure 4: Robustness evaluation of different methods under image degradation on GenImage.

4 Baseline Introduction

Below, we provide a brief introduction to each comparison method.

4.1 CNN-Based Mothed

CNNDetect (Wang et al. 2020) uses a ResNet-50 pre-trained on ImageNet and applies post-processing augmentations such as blurring and compression to enhance robustness.

DMID (Corvi et al. 2023) modifies ResNet-50 by removing the first down-sampling layer to preserve fine forensic details and applies stronger augmentation strategies.

LGrad (Tan et al. 2023) feeds a ResNet-50 with gradient-based artifact representations to capture generator-specific traces more effectively.

NPR (Tan et al. 2024a) inputs a residual image, computed as the difference between the original and its interpolated version, into ResNet-50 to highlight up-sampling artifacts.

DIRE (Wang et al. 2023) computes the reconstruction error from a generative model and uses it as input to a ResNet-50, exploiting the lower errors found in synthetic images.

4.2 CLIP-based Methods

DeFake (Sha et al. 2023) processes both images and prompts through the visual and textual encoders of CLIP, with the resulting features classified by a multilayer perceptron.

FatFormer (Liu et al. 2024) extends CLIP with forgery-aware adapters to extract spatial and frequency-domain cues and uses language-guided alignment for semantic consistency.

RINE (Koutlis and Papadopoulos 2024) uses intermediate features from a CLIP encoder and a trainable module to weight each layer’s contribution to the final decision.

C2P-CLIP (Tan et al. 2024b) fine-tunes CLIP’s image encoder using LoRA and applies contrastive learning guided by category prompts.

Head	Acc \uparrow
Classification	0.9099
Classification + ManiSeg	0.9190
Classification + AISeg	0.9226
Classification + ManiSeg + AISeg	0.9320

Table 4: Ablation study on segmentation heads.

Classification Label	Acc \uparrow	
	Copy-Move	Splicing
none	none	0.9027
1	1	0.8942
0	1	0.9104
1	0	0.9188
0	0	0.9205

Table 5: Ablation study on classification label. 0 indicates authentic, 1 indicates manipulated or AI-generated. none indicates only the COCO-Inpaint dataset is used for training.

4.3 VQA-based Methods

AntifakePrompt (Chang et al. 2023) employs the Instruct-BLIP VQA model with the fixed question “Is this photo real?” and uses soft prompt tuning to produce binary outputs.

4.4 Transformer-based Methods

CoDE (Baraldi et al. 2024) trains a Vision Transformer with a CLIP-like contrastive loss to separate real and fake image embeddings and pairs the model with a linear classifier.

BFree (Guillaro et al. 2025) uses inpainting for semantic alignment enhancement, making ViT pay more attention to the tampered parts to learn true and false features.

4.5 Hybrid or Patch-based Methods

LaDeDA (Cavia et al. 2024) divides the image into patches, classifies each patch individually, and averages the results to obtain the image-level prediction.

AIDE (Yan et al. 2025b)*- combines features from a ConvNeXt-based Open CLIP model with CNN features extracted from semantically filtered patches.

FasterThanLies (Lanzino et al. 2024) employs a Binary Neural Network for feature extraction, adds FFT magnitude and LBP images as auxiliary inputs, and uses a linear classifier for detection.

5 Experiments

5.1 Implementation Details

Vision Transformers (ViTs) (Dosovitskiy et al. 2021) have demonstrated superior performance over CNNs in manipulation segmentation tasks (Ma et al. 2024; Yan et al. 2025a). Accordingly, SegFormer-B2 (Xie et al. 2021) is adopted as

Training Dataset	Acc \uparrow
Inpainting	0.9063
Inpainting + Blended	0.9094
Inpainting + Copy-Move&Splicing	0.9205
Inpainting + Blended + Copy-Move&Splicing	0.9320

Table 6: Ablation study on manipulation diversity.

the backbone network. Both segmentation heads retain the original SegFormer structure, with the feature extractor initialized from the MiT-B2 weights pretrained on ImageNet. Given the large size of the original dataset, each epoch is trained on a randomly sampled 10% subset. The model is trained end-to-end using the binary cross-entropy loss function on NVIDIA A100 GPU. We use a batch size of 16 and set the learning rate to 1e-4. Early stopping is applied based on validation accuracy, with the delta and patience parameters set to 0.01 and 5, respectively.

As discussed in Section 1, resizing may distort subtle forensic traces, thereby compromising the generalization ability of the model. To mitigate this, RandomCrop and CenterCrop to 512×512 are applied during training and evaluation, respectively, following the strategy proposed in (Li et al. 2025). A padding of 1 pixel is applied in both cases. To avoid excessive padding on small images, test images smaller than 512×512 are resized prior to CenterCrop. Data augmentation follows the strategy proposed in (Wang et al. 2020), including label-preserving transformations such as blurring, color-jitter, flipping, and compression.

5.2 Generalization on GenImage

GenImage (Zhu et al. 2023) is a widely used benchmark containing images from eight generative models. Generated images are prompted from ImageNet’s 1,000 classes to ensure category-level semantic alignment. However, it contains inherent format-related biases, which we mitigate as described in the Format Alignment section. For evaluation, we randomly sample 1,000 generated and 1,000 authentic images per model for evaluation. Results are summarized in Table 2. Our method demonstrates strong generalization ability, surpassing the current state-of-the-art (Guillaro et al. 2025) by **5.8%** in accuracy. Notably, it achieves more consistent performance across different subsets of the benchmark, indicating that the model captures generalized features rather than overfitting to artifacts specific to individual generative models.

5.3 Generalization on Other Datasets

Given the recent popularity of GPT-4o Generated Images for its high-fidelity, we evaluate on three GPT-4o Generated Image datasets to test generalization. OpenAI-4o T2I Human Preference Dataset (Rapidata 2025) consists of 1v1 comparisons between GPT-4o and 12 other models. We randomly sample 1,000 for evaluation. ShareGPT-4o-Image (Chen et al. 2025) contains 45K text-to-image

Loss Components			Acc \uparrow
$\mathcal{L}_{\text{Cls.}}$	$\mathcal{L}_{\text{Seg}_{AI}}$	$\mathcal{L}_{\text{Seg}_{Ma}}$	
2	1	1	91.1
2	3	1	89.4
2	1	2	90.4
2	2	1	93.2

Table 7: Ablation study on three loss function components.

CrossAttn Config	Acc \uparrow
w/o CrossAttn	0.9183
CrossAttn	0.9058
Dual CrossAttn	0.9076
Reverse CrossAttn	0.9320

Table 8: Ablation study on CrossAttn.

and 46K text-and-image-to-image images. We randomly sample 1,000 from the former subset for evaluation. GPT-ImgEval (Yan et al. 2025d) contains 554 images generated by GPT-4o. An equal number of images from the ImageNet dataset were introduced as authentic images during evaluation. To further evaluate the generalization of GAMMA, we conduct experiments on four additional datasets. The results are summarized in Table 3. Our method attains the best performance on both benchmarks, reaching 99.1% accuracy on SynthWildX, which underscores its strong generalization and robustness across varied real and generative distributions. Competing methods exhibit severe degradation on the high-quality forgeries, exhibiting a pronounced tendency to label them as authentic. GAMMA remains robust because its artifact-decoupling segmentation head supplies fine-grained spatial awareness, and the reverse Cross-Attention mechanism corrects biases in the classification representation. Together these components prevent overconfidence on high-fidelity synthetic forgeries.

5.4 Robustness Under Degradations

In real-world scenarios, images transmitted online often undergo degradations which may erase critical forensic cues, especially under JPEG compression. Accordingly, we evaluate the robustness of the model under compression degradations. The results are illustrated in Figure 4, showing that GAMMA consistently achieves high performance.

5.5 Ablation Study

To thoroughly evaluate the effectiveness of each component in GAMMA, we conduct ablation studies on the GenImage dataset and GPT-4o datasets.

Segmentation Head. To analyze the effect of fine-grained supervision, we compare different segmentation head designs and evaluate their impact on model generalization, as shown in Tab. 4. Adding either ManiSeg or AISeg improves



Figure 5: Visualization of different manipulation types. Mask_AI and Mask_Mani respectively represent the Ground Truth of AI Seg. Head and Mani. Seg. Head. Inpainting, Inpainting-Blended, Copy-Move and Splicing respectively denote images that have undergone different types of manipulations on the source image.

classification accuracy, indicating their individual effectiveness. AISeg yields a higher gain than ManiSeg (+0.0127 vs. +0.0091). Combining both segmentation heads achieves the best performance, suggesting their complementary benefits. **Classification Label.** Image-level label definitions for manipulated images may significantly influence detection. We analyze how different labeling strategies impact model performance, result shown in Tab. 5. To avoid the impact of blended data, ablation studies are conducted only on the COCO-Inpaint training set. The baseline model without TampCOCO dataset achieves 90.27% accuracy. Direct supervision with both Copy-Move and Splicing labels (1,1) degrades performance to 89.42%. Treating all TampCOCO samples as real yields the best performance, indicating its manipulations are fundamentally different from AI-generated artifacts. TampCOCO does not synthesize new pixels but merely permutes existing ones, imposing structural inconsistencies that bias the model toward learning layout anomalies and thus enhances robustness in detecting AI-induced artifacts.

Manipulation Diversity. To validate the effectiveness of diverse manipulation strategies introduced in our framework, we perform an ablation study on their influence in the context of AI-generated image detection. The result are shown in Table 6, demonstrating that combining multiple manipulation types significantly enhances detection performance, confirming the benefit of diverse supervision signals.

Cross Attention. To further quantify the utility of Reverse Cross Attention, we performed an ablation study (Tab. 8). The result highlights that the choice of Query in Cross-Attention is critical. Naive CrossAttn (using the classification head as Query) and even Dual CrossAttn both degrade performance relative to the no-attention baseline (0.9058 and 0.9076 vs. 0.9183) implying that querying segmentation features with a biased classification signal induces confirmation bias and hurts generalization. In contrast, Reverse CrossAttn achieves the best accuracy (0.9320) by using segmentation-derived cues to attend into the classification branch. This directionality allows subtle generative artifacts captured in the segmentation branch to selectively reinforce and correct relevant components of the classification representation, effectively mitigating the intrinsic error tendencies of the classifier. The results validate the methodological insight that attention should be driven from the artifact-sensitive segmentation side back into classification, rather than the other way around.

Loss Ablation Study. Tab. 7 presents experimental results with various weight combinations of the loss terms. Experimental results show that increasing the AISeg weight is necessary, but excessive weighting impedes training and undermines primary detection performance.

6 Conclusions

Existing detectors generalize poorly because they depend on generation-specific artifacts. We propose GAMMA, which mitigates domain bias and enforces semantic alignment through diverse manipulations (e.g., inpainting-based edits and semantics-preserving perturbations), multi-task supervision with dual segmentation and classification heads

for fine-grained source attribution, and a reverse cross-attention module that lets the segmentation branches correct biased representations in the classifier. These components together force the model to rely less on superficial generation traces and more on underlying semantic consistency. GAMMA achieves state-of-the-art out-of-distribution generalization on the GenImage benchmark—improving accuracy by 5.8%—and stays robust to newly released generative models such as GPT-4o.

References

AI, M. 2024. Llama 3.2-Vision: Multimodal Large Language Model. Hugging Face Model Hub. Model release date: September 25, 2024.

Baraldi, L.; Cocchi, F.; Cornia, M.; Baraldi, L.; Nicolosi, A.; and Cucchiara, R. 2024. Contrasting Deepfakes Diffusion via Contrastive Learning and Global-Local Similarities. In *ECCV*.

Cavia, B.; Horwitz, E.; Reiss, T.; and Hoshen, Y. 2024. Real-Time Deepfake Detection in the Real-World. *arXiv preprint arXiv:2406.09398*.

Cazenavette, G.; Sud, A.; Leung, T.; and Usman, B. 2024. FakeInversion: Learning to Detect Images from Unseen Text-to-Image Models by Inverting Stable Diffusion. In *CVPR*, 10759–10769.

Chang, Y.-M.; Yeh, C.; Chiu, W.-C.; and Yu, N. 2023. AntifakePrompt: Prompt-Tuned Vision-Language Models are Fake Image Detectors. *arXiv preprint arXiv:2310.17419*.

Chen, B.; Zeng, J.; Yang, J.; and Yang, R. 2024a. DRCT: Diffusion Reconstruction Contrastive Training towards Universal Detection of Diffusion Generated Images. In Salakhutdinov, R.; Kolter, Z.; Heller, K.; Weller, A.; Oliver, N.; Scarlett, J.; and Berkenkamp, F., eds., *PMLR*, volume 235 of *Proceedings of Machine Learning Research*, 7621–7639. PMLR.

Chen, J.; Cai, Z.; Chen, P.; Chen, S.; Ji, K.; Wang, X.; Yang, Y.; and Wang, B. 2025. ShareGPT-4o-Image: Aligning Multimodal Models with GPT-4o-Level Image Generation. *arXiv preprint arXiv:2506.18095*.

Chen, Z.; Wang, W.; Tian, H.; Ye, S.; Gao, Z.; Cui, E.; Tong, W.; Hu, K.; Luo, J.; Ma, Z.; et al. 2024b. How far are we to gpt-4v? closing the gap to commercial multimodal models with open-source suites. *Science China Information Sciences*, 67(12): 220101.

Choi, Y.; Choi, M.; Kim, M.; Ha, J.-W.; Kim, S.; and Choo, J. 2018. StarGAN: Unified Generative Adversarial Networks for Multi-Domain Image-to-Image Translation. In *CVPR*.

Corvi, R.; Cozzolino, D.; Zingarini, G.; Poggi, G.; Nagano, K.; and Verdoliva, L. 2023. On The Detection of Synthetic Images Generated by Diffusion Models. In *ICASSP*, 1–5.

Deng, J.; Dong, W.; Socher, R.; Li, L.-J.; Li, K.; and Fei-Fei, L. 2009. ImageNet: A large-scale hierarchical image database. In *CVPR*, 248–255.

Dosovitskiy, A.; Beyer, L.; Kolesnikov, A.; Weissenborn, D.; Zhai, X.; Unterthiner, T.; Dehghani, M.; Minderer, M.;

Heigold, G.; Gelly, S.; Uszkoreit, J.; and Houlsby, N. 2021. An Image is Worth 16x16 Words: Transformers for Image Recognition at Scale. In *ICLR*.

Epstein, Z.; Hertzmann, A.; et al. 2023. Art and the science of generative AI. *Science*, 380(6650): 1110–1111.

Grommelt, P.; Weiss, L.; Pfreundt, F.-J.; and Keuper, J. 2025. Fake or JPEG? Revealing Common Biases in Generated Image Detection Datasets. In Del Bue, A.; Canton, C.; Pont-Tuset, J.; and Tommasi, T., eds., *ECCV Workshops*, 80–95. Cham: Springer Nature Switzerland. ISBN 978-3-031-92089-9.

Guillaro, F.; Zingarini, G.; Usman, B.; Sud, A.; Cozzolino, D.; and Verdoliva, L. 2025. A Bias-Free Training Paradigm for More General AI-generated Image Detection. In *CVPR*, 18685–18694.

Ho, J.; Jain, A.; and Abbeel, P. 2020. Denoising Diffusion Probabilistic Models. In Larochelle, H.; Ranzato, M.; Hadsell, R.; Balcan, M.; and Lin, H., eds., *NeurIPS*, volume 33, 6840–6851. Curran Associates, Inc.

Karageorgiou, D.; Papadopoulos, S.; Kompatsiaris, I.; and Gavves, E. 2025. Any-Resolution AI-Generated Image Detection by Spectral Learning. In *CVPR*, 18706–18717.

Karras, T.; Laine, S.; and Aila, T. 2019. A Style-Based Generator Architecture for Generative Adversarial Networks. In *CVPR*.

Kingma, D. P.; and Welling, M. 2014. Auto-Encoding Variational Bayes. In Bengio, Y.; and LeCun, Y., eds., *ICLR*.

Kirillov, A.; Mintun, E.; Ravi, N.; Mao, H.; Rolland, C.; Gustafson, L.; Xiao, T.; Whitehead, S.; Berg, A. C.; Lo, W. Y.; et al. 2023. Segment anything. In *ICCV*, 4015–4026.

Koutlis, C.; and Papadopoulos, S. 2024. Leveraging Representations from Intermediate Encoder-blocks for Synthetic Image Detection. In *ECCV*, 394–411.

Kwon, M.-J.; Nam, S.-H.; Yu, I.-J.; Lee, H.-K.; and Kim, C. 2022. Learning jpeg compression artifacts for image manipulation detection and localization. *IJCV*, 130(8): 1875–1895.

Lanzino, R.; Fontana, F.; Diko, A.; Marini, M. R.; and Cinque, L. 2024. Faster Than Lies: Real-time Deepfake Detection using Binary Neural Networks. In *CVPR Workshops*, 3771–3780.

Li, O.; Cai, J.; Hao, Y.; Jiang, X.; Hu, Y.; and Feng, F. 2025. Improving Synthetic Image Detection Towards Generalization: An Image Transformation Perspective. In Sun, Y.; Chierichetti, F.; Lauw, H. W.; Perlich, C.; Tok, W. H.; and Tomkins, A., eds., *KDD*, 2405–2414. ACM.

Lin, T.-Y.; Maire, M.; Belongie, S.; Hays, J.; Perona, P.; Ramanan, D.; Dollár, P.; and Zitnick, C. L. 2014. Microsoft COCO: Common Objects in Context. In Fleet, D.; Pajdla, T.; Schiele, B.; and Tuytelaars, T., eds., *ECCV*, 740–755. Cham.

Liu, H.; Li, C.; Wu, Q.; and Lee, Y. J. 2023. Visual Instruction Tuning. In *NeurIPS*.

Liu, H.; Tan, Z.; Tan, C.; Wei, Y.; Wang, J.; and Zhao, Y. 2024. Forgery-aware Adaptive Transformer for Generalizable Synthetic Image Detection. In *CVPR*, 10770–10780.

Ma, X.; Zhu, X.; Su, L.; Du, B.; Jiang, Z.; Tong, B.; Lei, Z.; Yang, X.; Pun, C.-M.; Lv, J.; and Zhou, J. 2024. IMDL-BenCo: A Comprehensive Benchmark and Codebase for Image Manipulation Detection & Localization. In Globereson, A.; Mackey, L.; Belgrave, D.; Fan, A.; Paquet, U.; Tomczak, J.; and Zhang, C., eds., *NeurIPS*, volume 37, 134591–134613. Curran Associates, Inc.

Open AI. 2025. Introducing 4o Image Generation. <https://openai.com/index/introducing-4o-image-generation/>. Accessed: 2025-07-21.

Radford, A.; Kim, J. W.; Hallacy, C.; Ramesh, A.; Goh, G.; Agarwal, S.; Sastry, G.; Askell, A.; Mishkin, P.; Clark, J.; et al. 2021. Learning transferable visual models from natural language supervision. In *ICML*, 8748–8763. PMLR.

Rapidata. 2025. OpenAI-4o T2I Human Preference. https://huggingface.co/datasets/Rapidata/OpenAI-4o_t2i_human_preference. Accessed: 2025-07-21.

Ricker, J.; Damm, S.; Holz, T.; and Fischer, A. 2024. Towards the Detection of Diffusion Model Deepfakes. In *VISAPP*, 446–457. INSTICC, SciTePress. ISBN 978-989-758-679-8.

Ricker, J.; Lukovnikov, D.; and Fischer, A. 2024. AEROBLADE: Training-Free Detection of Latent Diffusion Images Using Autoencoder Reconstruction Error. In *CVPR*, 9130–9140.

Rombach, R.; Blattmann, A.; Lorenz, D.; Esser, P.; and Ommer, B. 2022. High-Resolution Image Synthesis With Latent Diffusion Models. In *CVPR*, 10684–10695.

Sha, Z.; Li, Z.; Yu, N.; and Zhang, Y. 2023. DE-FAKE: Detection and Attribution of Fake Images Generated by Text-to-Image Generation Models. In *ACM SIGSAC*, 3418–3432.

Tan, C.; Liu, H.; Zhao, Y.; Wei, S.; Gu, G.; Liu, P.; and Wei, Y. 2024a. Rethinking the Up-Sampling Operations in CNN-based Generative Network for Generalizable Deepfake Detection. In *CVPR*.

Tan, C.; Tao, R.; Liu, H.; Gu, G.; Wu, B.; Zhao, Y.; and Wei, Y. 2024b. C2P-CLIP: Injecting Category Common Prompt in CLIP to Enhance Generalization in Deepfake Detection. *arXiv preprint arXiv:2408.09647*.

Tan, C.; Zhao, Y.; Wei, S.; Gu, G.; and Wei, Y. 2023. Learning on Gradients: Generalized Artifacts Representation for GAN-Generated Images Detection. In *CVPR*, 12105–12114.

Wang, P.; Bai, S.; Tan, S.; Wang, S.; Fan, Z.; Bai, J.; Chen, K.; Liu, X.; Wang, J.; Ge, W.; et al. 2024. Qwen2-vl: Enhancing vision-language model’s perception of the world at any resolution. *arXiv preprint arXiv:2409.12191*.

Wang, S.-Y.; Wang, O.; Zhang, R.; Owens, A.; and Efros, A. A. 2020. CNN-generated images are surprisingly easy to spot... for now. In *CVPR*, 8695–8704.

Wang, Y.; Huang, Z.; and Hong, X. 2025. OpenSDI: Spotting Diffusion-Generated Images in the Open World. In *CVPR*, 4291–4301.

Wang, Z.; Bao, J.; Zhou, W.; Wang, W.; Hu, H.; Chen, H.; and Li, H. 2023. DIRE for Diffusion-Generated Image Detection. In *ICCV*, 22445–22455.

Xiao, B.; Wu, H.; Xu, W.; Dai, X.; Hu, H.; Lu, Y.; Zeng, M.; Liu, C.; and Yuan, L. 2024. Florence-2: Advancing a unified representation for a variety of vision tasks. In *CVPR*, 4818–4829.

Xie, E.; Wang, W.; Yu, Z.; Anandkumar, A.; Alvarez, J. M.; and Luo, P. 2021. SegFormer: Simple and Efficient Design for Semantic Segmentation with Transformers. In Ranzato, M.; Beygelzimer, A.; Dauphin, Y.; Liang, P.; and Vaughan, J. W., eds., *NeurIPS*, volume 34, 12077–12090. Curran Associates, Inc.

Yan, H.; Hong, Y.; Zhan, J.; Ji, Y.; Lan, J.; Zhu, H.; Wang, W.; and Zhang, J. 2025a. COCO-Inpaint: A Benchmark for Image Inpainting Detection and Manipulation Localization. *arXiv preprint arXiv:2504.18361*.

Yan, S.; Li, O.; Cai, J.; Hao, Y.; Jiang, X.; Hu, Y.; and Xie, W. 2025b. A Sanity Check for AI-generated Image Detection. In *ICLR*.

Yan, Z.; Wang, J.; Jin, P.; Zhang, K.-Y.; Liu, C.; Chen, S.; Yao, T.; Ding, S.; Wu, B.; and Yuan, L. 2025c. Orthogonal Subspace Decomposition for Generalizable AI-Generated Image Detection. In *ICML*.

Yan, Z.; Ye, J.; Li, W.; Huang, Z.; Yuan, S.; He, X.; Lin, K.; He, J.; He, C.; and Yuan, L. 2025d. Gpt-imgeval: A comprehensive benchmark for diagnosing gpt4o in image generation. *arXiv preprint arXiv:2504.02782*.

Zhang, R.; Isola, P.; Efros, A. A.; Shechtman, E.; and Wang, O. 2018. The Unreasonable Effectiveness of Deep Features as a Perceptual Metric. In *CVPR*, 586–595.

Zhang, X.; Karaman, S.; and Chang, S.-F. 2019. Detecting and Simulating Artifacts in GAN Fake Images. In *WIFS*, 1–6.

Zhang, X.; Li, R.; Yu, J.; Xu, Y.; Li, W.; and Zhang, J. 2024. EditGuard: Versatile Image Watermarking for Tamper Localization and Copyright Protection. In *CVPR*, 11964–11974.

Zhu, M.; Chen, H.; YAN, Q.; Huang, X.; Lin, G.; Li, W.; Tu, Z.; Hu, H.; Hu, J.; and Wang, Y. 2023. GenImage: A Million-Scale Benchmark for Detecting AI-Generated Image. In Oh, A.; Naumann, T.; Globerson, A.; Saenko, K.; Hardt, M.; and Levine, S., eds., *NeurIPS*, volume 36, 77771–77782. Curran Associates, Inc.